



**Faculty of Manufacturing Engineering**

**MODELING OF REACTIVELY SPUTTERED TiAlN COATING ON  
TUNGSTEN CARBIDE INSERT TOOL: ITS PROPERTIES AND  
CUTTING PERFORMANCE IN DRY TURNING OF AISI D2 STEEL**

**Esmar Budi**

**Ph.D in Manufacturing Engineering**

**2010**

**MODELING OF REACTIVELY SPUTTERED TiAIN COATING ON TUNGSTEN  
CARBIDE INSERT TOOL: ITS PROPERTIES AND CUTTING PERFORMANCE  
IN DRY TURNING OF AISI D2 STEEL**

**ESMAR BUDI**

**A thesis submitted  
in fulfillment of the requirements for the degree of Doctor of Philosophy in  
Manufacturing Engineering**

**Faculty of Manufacturing Engineering**

**UNIVERSITI TEKNIKAL MALAYSIA MELAKA**

**2010**

## ABSTRACT

An extended theoretical model of reactive sputtering of TiAlN coating has been developed to study the effect of substrate bias ( $V_b$ ) and nitrogen ( $N_2$ ) flow rate on the coating composition and deposition rate. The model simulation results showed that the critical  $N_2$  flow rate ( $f_{N_2}^c$ ) to achieve a stoichiometry composition of unbiased ( $V_b = 0$  V) and biased ( $V_b = -80$  V) substrate was 4 sccm and 3 sccm, respectively. At  $N_2$  flow rate lower than  $f_{N_2}^c$ , the coating composition increased with an increase in  $V_b$  and  $N_2$  flow rate due to the increase of ion flux to the substrate while the deposition rate decreased due to the coating densification and the decreased sputtering rate. At  $N_2$  flow rate higher than  $f_{N_2}^c$ , the coating composition and deposition rate did not depend on the  $V_b$  and  $N_2$  flow rate due to the domination of neutral particles deposition than ions deposition. The model verification using secondary data showed an accurately prediction on the coating composition and deposition rate at  $N_2$  flow rate higher than  $f_{N_2}^c$ . The calculated coating composition at  $N_2$  flow rate lower than  $f_{N_2}^c$  showed a deviation due to heterogeneous reactions between the sputtered particles (Ti and Al) and N at the substrate surface, while the deviation of calculated deposition rate was due to coating densification. The experimental investigation was designed by using Response Surface Methodology (RSM) and conducted by using magnetron sputtering in deposition of TiAlN coating on WC inserts. The coating composition and thickness were obtained by using SEM/EDX. The coating structure and morphology were obtained by using XRD and AFM, respectively. The coating hardness and adhesion were obtained by using ultra-micro hardness test and indentation test, respectively. The cutting test was carried out in CNC dry turning of AISI D2 steel. The flank wear and surface roughness were obtained by using optical microscopy and surface roughness tester, respectively. The results showed that generally the coating composition of biased substrate (-100, -150, -200 V) was consistently higher than that of unbiased substrate whereas the deposition rate of biased substrate is lower than that of unbiased substrate. Analysis of the coating thickness showed that generally the coating thickness decreased with an increase in the  $V_b$  and  $N_2$  flow rate. At  $N_2$  flow rate lower than 50 sccm, the thinnest coating ( $\sim 1000$  nm) is achieved by unbiased substrate due to low ions fluxes for reaction at the substrate surface. The coating hardness, structure and morphology were significantly influenced by the  $V_b$  while the interaction of the  $V_b$  and  $N_2$  flow rate significantly influenced the coating adhesion. The coating hardness increased ( $\sim 7$  GPa) with an increase in the  $V_b$  up to -200 V due to decreased coating crystal size. At  $N_2$  flow rate of 70 sccm, the adhesion strength increased with an increase in the  $V_b$  up to -200 V due to decreased compressive stress. The lowest flank wear ( $\sim 0.4$  mm) due to high adhesion strength was achieved at -200 V and 70 sccm.

## ABSTRAK

Sebuah model percikan reaktif salutan TiAlN lanjut telah dibangunkan untuk kajian kesan pincangan substrat ( $V_b$ ) dan kadar aliran nitrogen ( $N_2$ ) pada kandungan salutan dan kadar pengendapan. Hasil simulasi model menunjukkan bahawa kadar aliran  $N_2$  genting ( $f_{N_2}^c$ ) substrat tak terpinang ( $V_b = 0$  V) dan terpinang ( $V_b = -80$  V) untuk mencapai kandungan stoikiometri masing-masing adalah 4 sccm dan 3 sccm. Pada kadar aliran  $N_2$  kurang daripada  $f_{N_2}^c$ , kandungan salutan bertambah dengan penambahan  $V_b$  disebabkan penambahan fluks ion ke permukaan substrat, sedangkan kadar pengendapan berkurang disebabkan penempatan salutan dan pengurangan kadar percikan. Pada kadar aliran  $N_2$  di atas  $f_{N_2}^c$ , kandungan salutan dan kadar pengendapan tidak bergantung pada  $V_b$  dan kadar aliran  $N_2$ , disebabkan penguasaan pengendapan zarah neutral daripada pengendapan ion. Pengesahan model dengan menggunakan data sekunder menunjukkan jangkaan jitu kandungan salutan dan kadar pengendapan pada kadar aliran  $N_2$  di atas  $f_{N_2}^c$ . Kandungan salutan jangkaan pada kadar aliran  $N_2$  di bawah  $f_{N_2}^c$ , menunjukkan sebuah sisihan disebabkan tindak balas heterogen antara zarah percik (Ti dan Al) dan N pada permukaan substrat, sementara itu sisihan kadar pengendapan jangkaan disebabkan penempatan salutan. Ujikaji dirancang dengan menggunakan kaedah permukaan gerak balas (RSM) dan dilaksanakan dengan menggunakan percikan magnetron dalam pengendapan salutan TiAlN pada sisip WC. Kandungan dan ketebalan salutan diperolehi dengan SEM/EDX. Struktur dan morfologi salutan masing-masing diperolehi dengan XRD dan AFM. Kekerasan dan lekatan salutan masing-masing diperolehi dengan ujian kekerasan mikro ultra dan ujian lekuk. Ujian pemotongan dilaksanakan dengan larik CNC pada keluli AISI D2. Keausan sisi dan kekasaran permukaan masing-masing diperolehi dengan menggunakan mikroskop optik dan ujian kekasaran permukaan. Hasil kajian menunjukkan bahawa pada umumnya kandungan salutan substrat terpinang (-100, -150, -200 V) adalah tebal lebih tinggi daripada kandungan substrat tak terpinang sebaliknya kadar pengendapan substrat terpinang adalah lebih rendah daripada kadar pengendapan substrat tak terpinang. Analisis pada ketebalan salutan menunjukkan bahawa umumnya, ketebalan salutan berkurang dengan penambahan  $V_b$  dan kadar aliran  $N_2$ . Sungguhpun begitu pada kadar aliran  $N_2$  di bawah 50 sccm, ketebalan salutan paling nipis (~1000 nm) dicapai oleh substrat tak terpinang disebabkan fluks ion yang rendah untuk tindak balas pada permukaan substrat. Kekerasan, struktur dan morfologi salutan adalah dipengaruhi secara signifikan oleh  $V_b$ , sementara saling tindak antara  $V_b$  dan kadar aliran  $N_2$  mempengaruhi lekatan salutan. Pada umumnya, kekerasan salutan bertambah (~7 GPa) dengan penambahan  $V_b$  kepada -200 V disebabkan pengurangan saiz hablur. Pada kadar aliran  $N_2$  70 sccm, kekuatan lekatan bertambah dengan penambahan  $V_b$  kepada -200 V disebabkan pengurangan tegangan mampat. Keausan sisi terendah (~0.4 mm) yang disebabkan kekuatan lekatan tinggi dicapai pada -200 V dan 70 sccm.

## ACKNOWLEDGEMENTS


The author would like to express sincere appreciation to Prof. Dr. Mohd. Razali bin Muhamad, my principal supervisor, for guiding and giving inputs to the present work. I am very thankful to En. Saifudin Hafiz bin Yahaya, my co-supervisor, for his contribution in the model development and to Dr. Md Nizam bin Abdul Rahman for very valuable discussions and advice during the course at my study.

I gratefully acknowledge the support from the staff at the Advanced Manufacturing Center (AMC), CNC, Metrology and Material Engineering Laboratory during the experimental work. I am also grateful to Faculty of Manufacturing Engineering and Universiti Teknikal Malaysia Melaka (UTeM) for providing research facilities and funds and I would like to thank Physics Department and Universitas Negeri Jakarta (UNJ) for their approval and support during study leave.

Thank you to my colleagues, postgraduate students and staff of UTeM. Finally, I am very grateful to my family, wife and children, for their patience and support.

## DECLARATION

I declare that this thesis entitled “Modeling of reactively sputtered TiAlN coating on tungsten carbide insert tool: its properties and cutting performance in dry turning of AISI D2 steel” is the result of my own research except as cited in the references. The thesis has not been accepted for any degree and is not concurrently submitted in candidature of any other degree.

Signature :  .....

Name : ESMAK BUDI .....

Date : 10 Mei 2010 .....

## **DEDICATION**

To my beloved father, mother, wife and children:  
Sumarna (alm.), Komariah, Pepi, Giga and Tera

## TABLE OF CONTENT

|                              | <b>PAGE</b> |
|------------------------------|-------------|
| <b>ABSTRACT</b>              | ii          |
| <b>ABSTRAK</b>               | iii         |
| <b>ACKNOWLEDGEMENTS</b>      | iv          |
| <b>DECLARATION</b>           | v           |
| <b>DEDICATION</b>            | vi          |
| <b>TABLE OF CONTENT</b>      | vii         |
| <b>LIST OF TABLES</b>        | xii         |
| <b>LIST OF FIGURES</b>       | xvi         |
| <b>LIST OF ABBREVIATIONS</b> | xxiv        |
| <b>LIST OF SYMBOLS</b>       | xxv         |
| <b>LIST OF APPENDICES</b>    | xxix        |
| <b>RELATED PUBLICATIONS</b>  | xxx         |

### CHAPTER

|          |   |           |
|----------|---|-----------|
| <b>1</b> | <b>INTRODUCTION</b>                     | <b>1</b>  |
|          | 1.1 Background                          | 1         |
|          | 1.2 Research problem                    | 4         |
|          | 1.3 Objectives of study                 | 7         |
|          | 1.4 Significance of research            | 7         |
|          | 1.5 Scope of research                   | 10        |
|          | 1.6 Structure of thesis                 | 11        |
| <b>2</b> | <b>LITERATURE REVIEW</b>                | <b>12</b> |
|          | 2.1 Reactive sputtering process         | 12        |
|          | 2.2 Sputtering parameters               | 17        |
|          | 2.2.1 Sputtering yield                  | 17        |
|          | 2.2.2 Sticking coefficient              | 18        |
|          | 2.2.3 Reactive gas flow                 | 19        |
|          | 2.2.4 Vacuum pumping and pressure       | 20        |
|          | 2.2.5 Substrate bias                    | 22        |
|          | 2.2.6 Substrate temperature             | 23        |
|          | 2.2.7 Target power, voltage and current | 23        |



|          |  |           |
|----------|--|-----------|
| 2.3      | TiAlN coating properties   | 24        |
| 2.3.1    | Hardness   | 24        |
| 2.3.2    | Adhesion   | 29        |
| 2.3.3    | Residual stress  | 31        |
| 2.3.4    | Composition  | 33        |
| 2.3.5    | Structure and morphology   | 33        |
| 2.3.6    | Crystal orientation  | 37        |
| 2.3.7    | Coating thickness  | 41        |
| 2.4      | Effect of reactive sputtering parameters on TiAlN coating properties   | 42        |
| 2.4.1    | Effect of nitrogen flow rate   | 42        |
| 2.4.2    | Effect of nitrogen pressure  | 43        |
| 2.4.3    | Effect of substrate bias   | 45        |
| 2.4.4    | Effect of substrate temperature  | 48        |
| 2.4.5    | Effect of sputtering power   | 49        |
| 2.4.6    | Effect of substrate rotation   | 50        |
| 2.4.7    | Hysteresis effect  | 51        |
| 2.5      | Modeling of sputtering process   | 52        |
| 2.6      | Experimental design of sputtering process                              | 56        |
| 2.7      | Cutting tool performance   | 57        |
| 2.7.1    | Tool wear  | 57        |
| 2.7.2    | Tool material  | 59        |
| 2.7.3    | Work material  | 60        |
| 2.7.4    | Surface roughness  | 61        |
| 2.8      | Effect of cutting parameters on cutting performance                    | 63        |
| 2.8.1    | Effect of cutting parameters on tool wear                              | 64        |
| 2.8.2    | Effect of cutting parameters on surface roughness                      | 66        |
| 2.9      | Summary  | 70        |
| <b>3</b> | <b>MODEL OF REACTIVE SPUTTERING</b>                                    | <b>72</b> |
| 3.1      | Plasma sheath potential and ion flux                                   | 73        |
| 3.2      | Ion and neutral particles flux in reactive sputtering of TiAlN coating | 79        |
| 3.3      | Total particle fluxes in reactive sputtering                           | 81        |
| 3.3.1    | Reactions at target  | 83        |
| 3.3.2    | Reactions at substrate   | 85        |
| 3.4      | Kinetic of the reactive gas  | 90        |
| 3.5      | Sputtering and deposition rate   | 91        |
| 3.6      | Sensitivity analysis   | 92        |
| <b>4</b> | <b>EXPERIMENTAL INVESTIGATION</b>                                      | <b>94</b> |
| 4.1      | Response Surface Methodology   | 94        |
| 4.1.1    | Center Composite Design  | 97        |
| 4.1.2    | Experimental design and analysis                                       | 99        |
| 4.2      | Experiment procedure   | 100       |
| 4.2.1    | Preliminary experiment of TiAlN coating deposition                     | 101       |
| 4.2.2    | Experiment of TiAlN coating deposition                                 | 101       |
| 4.2.2.1  | Substrate  | 102       |
| 4.2.2.2  | Sputtering parameters  | 102       |
| 4.2.2.3  | Machine of sputtering system   | 103       |

|          |   |            |
|----------|---|------------|
| 4.2.2.4  | Procedures of TiAlN coating deposition                                  | 104        |
| 4.2.3    | Cutting performance test  | 105        |
| 4.2.3.1  | Tool and work material  | 105        |
| 4.2.3.2  | Cutting condition   | 108        |
| 4.3      | Characterization of coating surface and its performance                 | 108        |
| 4.3.1    | Optical microscopy  | 109        |
| 4.3.2    | Surface roughness test  | 109        |
| 4.3.3    | Scanning Electron Microscopy (SEM)<br>and Energy Dispersive X-Ray (EDX) | 110        |
| 4.3.4    | X-Ray Diffraction (XRD)   | 111        |
| 4.3.5    | Adhesion test   | 113        |
| 4.3.6    | Ultra-micro hardness test   | 113        |
| 4.3.7    | Atomic Force Microscopy (AFM)   | 114        |
| <b>5</b> | <b>RESULTS AND DISCUSSIONS</b>  | <b>115</b> |
| 5.1      | Model simulation results  | 116        |
| 5.1.1    | Effect of substrate bias at various nitrogen flow rate                  | 118        |
| 5.1.2    | Effect of pump speed and target current                                 | 120        |
| 5.1.3    | Sensitivity analysis on reactive sputtering model                       | 122        |
| 5.1.4    | Comparison with secondary data  | 129        |
| 5.1.5    | Discussion  | 139        |
| 5.2      | Preliminary experiment of sputtering deposition                         | 145        |
| 5.3      | Experimental result of sputtered TiAlN coating                          | 147        |
| 5.3.1    | Composition of TiAlN coating  | 147        |
| 5.3.1.1  | Analysis of TiAlN coating composition                                   | 153        |
| 5.3.1.2  | Analysis of TiAlN coating composition<br>using RSM                      | 157        |
| A.       | Analysis of Ti/Al ratio   | 158        |
| B.       | Analysis of Ti/(Ti+Al+N) ratio  | 162        |
| 5.3.1.3  | Discussion  | 166        |
| 5.3.2    | Deposition rate   | 168        |
| 5.3.2.1  | Effect of substrate bias on TiAlN coating<br>thickness                  | 173        |
| 5.3.2.2  | Effect of nitrogen flow rate on TiAlN coating<br>thickness              | 177        |
| 5.3.2.3  | Discussion  | 182        |
| 5.3.3    | Structure of TiAlN coating  | 185        |
| 5.3.3.1  | Substrate (tungsten carbide insert)                                     | 185        |
| 5.3.3.2  | Effect of substrate bias on TiAlN coating<br>structure                  | 186        |
| 5.3.3.3  | Effect of nitrogen flow rate on TiAlN coating<br>Structure              | 193        |
| 5.3.3.4  | Analysis of TiAlN coating structure using RSM                           | 200        |
| A.       | Analysis of crystal plane spacing of (111)<br>TiAlN coating             | 201        |
| B.       | Analysis of crystal size of (111)<br>TiAlN coating                      | 205        |
| 5.3.3.5  | Discussion  | 210        |

|         |  |     |
|---------|--|-----|
| 5.3.4   | Morphology of TiAlN coating  | 212 |
| 5.3.4.1 | Effect of substrate bias on TiAlN coating roughness                  | 213 |
| 5.3.4.2 | Effect of nitrogen flow rate on TiAlN coating roughness              | 217 |
| 5.3.4.3 | Analysis of TiAlN coating roughness using RSM                        | 221 |
| 5.3.4.4 | Discussion   | 226 |
| 5.3.5   | Hardness of TiAlN coating  | 229 |
| 5.3.5.1 | Effect of substrate bias on TiAlN coating hardness                   | 230 |
| 5.3.5.2 | Effect of nitrogen flow rate on TiAlN coating hardness               | 232 |
| 5.3.5.3 | Analysis of TiAlN coating hardness using RSM                         | 235 |
| 5.3.5.4 | Discussion   | 239 |
| 5.3.6   | Adhesion of TiAlN coating  | 243 |
| 5.3.6.1 | Effect of substrate bias on TiAlN coating adhesion                   | 244 |
| 5.3.6.2 | Effect of nitrogen flow rate on TiAlN coating adhesion               | 246 |
| 5.3.6.3 | Analysis of TiAlN coating adhesion using RSM                         | 249 |
| 5.3.6.4 | Discussion   | 255 |
| 5.4     | Study of cutting parameters optimization using RSM                   | 256 |
| 5.4.1   | Analysis of cutting parameters effect on flank wear                  | 258 |
| 5.4.2   | Analysis of cutting parameters effect on surface roughness           | 265 |
| 5.4.3   | Optimization of flank wear and surface roughness                     | 272 |
| 5.4.4   | Discussion   | 273 |
| 5.5     | Cutting performance of TiAlN coating                                 | 275 |
| 5.5.1   | Analysis of sputtering parameters effect on TiAlN coating flank wear | 276 |
| 5.5.1.1 | Effect of substrate bias on TiAlN coating flank wear                 | 276 |
| 5.5.1.2 | Effect of nitrogen flow rate on TiAlN coating flank wear             | 278 |
| 5.5.2   | Analysis of TiAlN coating flank wear using RSM                       | 281 |
| 5.5.3   | Analysis of surface roughness using RSM                              | 284 |
| 5.5.4   | Comparison of TiAlN coating performance                              | 286 |
| 5.5.5   | Discussion   | 287 |
| 5.6     | Summary of the results   | 289 |
| 5.6.1   | Correlation of TiAlN coating properties and its cutting performance  | 289 |
| 5.6.2   | Correlation of TiAlN coating properties                              | 296 |

|          |                                    |            |
|----------|------------------------------------|------------|
| <b>6</b> | <b>CONCLUSIONS AND FUTURE WORK</b> | <b>303</b> |
| 6.1      | Conclusions                        | 304        |
| 6.2      | Future work                        | 306        |
|          | <b>REFERENCES</b>                  | <b>308</b> |
|          | <b>APPENDICES</b>                  | <b>338</b> |

## LIST OF TABLES

| TABLE | TITLE  | PAGE |
|-------|--|------|
| 2.1   | Al content (x), structure/phase and hardness of Ti <sub>1-x</sub> Al <sub>x</sub> N coating  | 28   |
| 2.2   | Al content (x), structure/phase and preferred plan orientation of Ti <sub>1-x</sub> Al <sub>x</sub> N coating  | 41   |
| 2.3   | W-Co substrate used in several investigations  | 60   |
| 4.1   | Sputtering parameters for preliminary experiment of TiAlN coating  | 101  |
| 4.2   | Sputtering parameters of TiAlN coating deposition  | 103  |
| 4.3   | Material specifications  | 106  |
| 4.4   | Workpiece chemical composition   | 106  |
| 4.5   | Cutting parameters   | 108  |
| 5.1   | Relative error of surface coverage fraction on substrate ( $\theta_s$ ) of TiAlN coating with respect to data of Lii et al. (1998) at I = 0.7 A, $V_b = -80$ V and S = 100 l/s | 131  |
| 5.2   | Relative error of deposition rate of TiAlN coating with respect to data of Lii et al. (1998) at I = 0.7 A, $V_b = -80$ V, S = 100 l/s  | 133  |
| 5.3   | Relative error of model calculated $\theta_s$ of TiAlN coating with respect to data of Shew et al. (1997) at I = 0.7 A, $V_b = 0$ and S = 100 l/s                              | 135  |
| 5.4   | Relative error of model calculated $\theta_s$ of TiAlN coating with respect to data of Shew et al. (1997) at I = 0.7 A, $V_b = -80$ V and S = 100 l/s                          | 135  |

|      |  |     |
|------|--|-----|
| 5.5  | Relative error of model calculated deposition rate of TiAlN coating with respect to data of Shew et al. (1997) at $I = 0.7$ A, $V_b = 0$ V and $S = 100$ l/s   | 138 |
| 5.6  | Relative error of model calculated deposition rate of TiAlN coating with respect to data of Shew et al. (1997) at $I = 0.7$ A, $V_b = -80$ V and $S = 100$ l/s | 138 |
| 5.7  | Experimental result of TiAlN coating composition and surface coverage fraction on substrate ( $\theta$ ) at $I = 5$ A and $S = 2050$ l/s                       | 148 |
| 5.8  | Relative error of $\theta_s$ of TiAlN coating at $I = 5$ A and $S = 2050$ l/s  | 152 |
| 5.9  | Experimental result of Ti/Al and Ti/(Ti+Al+N) ratio of TiAlN coating using RSM   | 157 |
| 5.10 | Sequential model sum of squares of Ti/Al ratio   | 158 |
| 5.11 | Lack of fit tests of Ti/Al ratio   | 158 |
| 5.12 | ANOVA for response surface 2FI model analysis of Ti/Al ratio   | 159 |
| 5.13 | Sequential model sum of squares of Ti/(Ti+Al+N) ratio  | 162 |
| 5.14 | Lack of fit tests of Ti/(Ti+Al+N) ratio  | 162 |
| 5.15 | ANOVA for response surface quadratic model analysis of Ti/(Ti+Al+N) ratio  | 163 |
| 5.16 | Experimental result of model calculated $D$ of TiAlN coating at $I = 5$ A and $S = 2050$ l/s   | 169 |
| 5.17 | Relative error of model calculated deposition rate of TiAlN coating at $I = 5$ A and $S = 2050$ l/s  | 172 |
| 5.18 | XRD data of TiAlN coating at various nitrogen flow rate and substrate bias   | 193 |
| 5.19 | XRD data of TiAlN coating at various substrate bias and nitrogen flow rate   | 200 |
| 5.20 | Experimental result of $D_{111}$ and $d_{111}$ of TiAlN coating using RSM  | 201 |
| 5.21 | Sequential model sum of squares of $d_{111}$   | 202 |
| 5.22 | Lack of fit tests of $d_{111}$   | 202 |
| 5.23 | ANOVA for response surface linear model of $d_{111}$   | 203 |
| 5.24 | Sequential model sum of squares of $D_{111}$   | 205 |

|      |  |     |
|------|--|-----|
| 5.25 | Lack of fit tests of $D_{111}$   | 205 |
| 5.26 | ANOVA for response surface linear model of $D_{111}$   | 206 |
| 5.27 | Confirmation test results of $d_{111}$   | 209 |
| 5.28 | Experimental result of TiAlN coating roughness   | 213 |
| 5.29 | Experimental result of rms roughness of TiAlN coating using RSM                              | 222 |
| 5.30 | Sequential model sum of squares of rms roughness   | 223 |
| 5.31 | Lack of fit test of rms roughness  | 223 |
| 5.32 | ANOVA for response surface linear model of rms roughness                                     | 224 |
| 5.33 | Experimental result of TiAlN coating hardness  | 230 |
| 5.34 | Experimental result of TiAlN coating hardness using RSM                                      | 235 |
| 5.35 | Sequential model sum of squares of TiAlN coating hardness                                    | 236 |
| 5.36 | Lack of fit test of TiAlN coating hardness   | 236 |
| 5.37 | ANOVA for response surface quadratic model of TiAlN coating hardness                         | 237 |
| 5.38 | Experimental result of lateral crack diameter measurement of TiAlN coating                   | 244 |
| 5.39 | Experimental result of lateral crack diameter and slope of TiAlN coating using RSM           | 249 |
| 5.40 | Sequential model sum of squares of slope   | 250 |
| 5.41 | Lack of fit test of slope  | 250 |
| 5.42 | ANOVA for response surface quadratic model of slope  | 251 |
| 5.43 | Confirmation test results of slope   | 254 |
| 5.44 | Experimental result of commercially TiAlN coating flank wear and surface roughness using RSM | 257 |
| 5.45 | Sequential model sum of squares of commercially TiAlN coating flank wear                     | 258 |
| 5.46 | Lack of fit test of commercially TiAlN coating flank wear                                    | 259 |
| 5.47 | ANOVA for response surface quadratic model of commercially TiAlN coating flank wear          | 260 |
| 5.48 | Confirmation test results of commercially TiAlN coating flank wear                           | 265 |
| 5.49 | Sequential model sum of squares of surface roughness   | 265 |
| 5.50 | Lack of fit test of surface roughness  | 266 |

|      |  |     |
|------|--|-----|
| 5.51 | ANOVA for response surface linear model of surface roughness                                   | 266 |
| 5.52 | Confirmation test results of surface roughness   | 272 |
| 5.53 | Experimental result of flank wear and surface roughness of TiAlN coating performance using RSM | 276 |
| 5.54 | Sequential model sum of squares of flank wear of TiAlN coating                                 | 281 |
| 5.55 | Lack of fit test of flank wear of TiAlN coating  | 282 |
| 5.56 | ANOVA for response surface linear model of flank wear of TiAlN coating                         | 282 |
| 5.57 | ANOVA for the effect of sputtering parameters on surface roughness                             | 285 |
| 5.58 | Comparison of flank wear and surface roughness   | 286 |



## LIST OF FIGURES

| FIGURE | TITLE  | PAGE |
|--------|--|------|
| 2.1    | Schematic diagram of reactive sputtering (Berg and Nyberg, 2005)   | 13   |
| 2.2    | Schematic diagram of sputtered target (Mattox, 1998)   | 14   |
| 2.3    | Schematic diagram of molecules adsorption on a flat surface (Ohtsu et al., 2007)   | 15   |
| 2.4    | TiAlN structure (fcc-NaCl structure) models schematic. Ti occupies fcc positions and the cube corners. Al occupy the octahedral sites at the centers of the cube edges (Paldey et al., 2004)                         | 34   |
| 2.5    | Model schematic of (a) hexagonal-TiAlN; (b) hexagonal-AlN (Kimura et al., 2003)  | 35   |
| 2.6    | Thornton structure zone model. Zone I, II, III and T are related to growth mechanism of atomic shadowing during transport, surface diffusion, bulk diffusion and transition of I & II, respectively (Thornton, 1986) | 36   |
| 2.7    | Structure Zone Model at various coating thickness as function of reduced temperature $T_s/T_m$ , where $T_s$ = deposition temperature and $T_m$ = melting point of the material (Barna & Adamik, 1998)               | 38   |
| 2.8    | Region of wear at major and minor cutting edge in single point turning tool (Boothroyd & Knight, 2006)   | 58   |
| 2.9    | (a) Region of tool wear on cutting tool; (b) flank wear measurement (Lim et al., 1999)   | 59   |
| 2.10   | Schematic diagram of surface roughness (Lou et al., 1998)  | 62   |
| 2.11   | Schematic diagram of surface roughness measurement   | 63   |
| 3.1.   | Schematic diagram of the reactive gas flow in reactive sputtering process based on Berg's model (Berg et al., 1987)  | 73   |

|     |  |     |
|-----|--|-----|
| 3.2 | (a) Formation of plasma sheaths and plasma sheath potential due to the existing of a difference in potential between $V_p$ and $V_b$ ; (b) potential drop (from $V_p$ to $-V_b$ ) within the plasma sheath increase with an increase in negatively $V_b$ (note: $ V_{b1}  <  V_{b2} $ ) (Lieberman & Lichtenberg, 1994; Ellmer, 2000; Zhou et.al., 2007) | 74  |
| 3.3 | Schematic diagram of total particle fluxes at target and substrate.  | 82  |
| 3.4 | Schematic diagram of total particle fluxes at target   | 83  |
| 3.5 | Schematic diagram of total particle fluxes at substrate  | 86  |
| 4.1 | Central Composite Design for 3 factors at two levels   | 95  |
| 4.2 | Examples of response surface in: (a) contour plot; (b) three dimension; (c) cubic surface; where $x_1, x_2, x_3$ are independent variables (Design expert, 2006)   | 96  |
| 4.3 | Experimental design flow   | 100 |
| 4.4 | Schematic diagram of magnetron sputtering system (top view)  | 104 |
| 4.5 | Schematic diagram of WC insert tool  | 107 |
| 4.6 | Schematic diagram of tool holder: (a) tool holder 1; (b) tool holder 2   | 107 |
| 4.7 | Measurement of flank wear, VC (ISO 3685 (E), 1993)   | 109 |
| 4.8 | Schematic diagram of signal produced and penetration depth of incident electron beam with the sample (Mattox, 1998)  | 111 |
| 5.1 | Simulation results of TiAlN coating at $I = 0.7$ A, $S = 100$ l/s, $V_b = 0$ and various nitrogen flow rate: (a) surface coverage fraction on target ( $\theta_t$ ) and substrate ( $\theta_s$ ); (b) deposition rate; (c) nitrogen flow consumption by target ( $F_t$ ), substrate ( $F_s$ ) and pump ( $F_p$ )   | 117 |
| 5.2 | Simulation results of TiAlN coating at $I = 0.7$ A, $S = 100$ l/s and various substrate bias and nitrogen flow rate: (a) surface coverage fraction on target ( $\theta_t$ ) and substrate ( $\theta_s$ ); (b) deposition rate; (c) nitrogen flow consumption by target ( $F_t$ ), substrate ( $F_s$ ) and pump ( $F_p$ )                                 | 119 |
| 5.3 | Simulation results of TiAlN coating at $I = 0.7$ A, $V_b = -80$ V and various pump speed and nitrogen flow rate: (a) surface coverage fraction on substrate ( $\theta_s$ ); (b) deposition rate  | 120 |
| 5.4 | Simulation results of TiAlN coating at $V_b = -80$ V, $S = 2050$ l/s and various target current and nitrogen flow rate: (a) surface coverage fraction on substrate ( $\theta_s$ ); (b) deposition rate   | 121 |

|      |  |     |
|------|--|-----|
| 5.5  | Sensitivity analysis of: (a), (b) surface coverage fraction on substrate ( $\theta_s$ ); (c) deposition rate (D) at $I = 0.7$ A, $S = 100$ l/s and various nitrogen flow rate and substrate bias   | 123 |
| 5.6  | Sensitivity analysis of: (a) surface coverage fraction on substrate ( $\theta_s$ ); (b) deposition rate (D) at $I = 0.7$ A, $S = 100$ l/s and various substrate bias and nitrogen flow rate  | 125 |
| 5.7  | Sensitivity analysis of: (a) surface coverage fraction on substrate ( $\theta_s$ ); (b) deposition rate (D) at $I = 5$ A, $S = 2050$ l/s and various nitrogen flow rate and substrate bias   | 127 |
| 5.8  | Sensitivity analysis of: (a) surface coverage fraction on substrate ( $\theta_s$ ); (b) deposition rate (D) at $I = 5$ A, $S = 2050$ l/s and various substrate bias and nitrogen flow rate   | 128 |
| 5.9  | Model calculated (solid line) and measured $\theta_s$ of TiAlN coating at $I = 0.7$ A, $S = 100$ l/s, $V_b = -80$ V and various nitrogen flow rate:<br>(a) Auger Electron Spectroscopy (AES) analysis;<br>(b) Wave-Length Dispersive x-ray spectroscopy (WDS) analysis | 130 |
| 5.10 | Model calculated (solid line) and measured deposition rate of TiAlN coating (data of Lii et al., 1998) at $I = 0.7$ A, $S = 100$ l/s, $V_b = -80$ V and various nitrogen flow rate   | 132 |
| 5.11 | Model calculated (solid line) and measured $\theta_s$ (data of Shew et al., 1997) of TiAlN coating at $I = 0.7$ A, $S = 100$ l/s and various nitrogen flow rate:<br>(a) $V_b = 0$ ; (b) $V_b = -80$ V  | 134 |
| 5.12 | Model calculated (solid line) and measured deposition rate of TiAlN coating (data of Shew et al., 1997) at $I = 0.7$ A, $S = 100$ l/s and various nitrogen flow rate and substrate bias of:<br>(a) $V_b = 0$ , (b) $V_b = -80$ V                                       | 137 |
| 5.13 | Simulation result for $N_2$ partial pressure during TiAlN coating deposition at $I = 0.7$ A, $S = 100$ l/s, $V_b = -80$ V and various nitrogen flow rate   | 140 |
| 5.14 | SEM of TiAlN coating on WC insert at $I = 3$ A, $V_b = -100$ V, $T = 350$ °C, substrate rotation = 5 rpm, $t = 90$ min, Ar flow rate = 123 sccm, $N_2$ flow rate of:<br>(a) 20 sccm; (b) 10 sccm   | 145 |
| 5.15 | EDX of TiAlN coating on WC insert at $I = 3$ A, $V_b = -100$ V, $T = 350$ °C, substrate rotation = 5 rpm, $t = 90$ min, Ar flow rate = 123 sccm, $N_2$ flow rate of:<br>(a) 20 sccm, (b) 10 sccm   | 146 |
| 5.16 | SEM of TiAlN coating on WC insert at $I = 5$ A, $V_b = -100$ V, $T = 350$ °C, substrate rotation = 5 rpm, $t = 90$ min, Ar flow rate = 123 sccm, $N_2$ flow rate = 60 sccm   | 147 |

|      |   |     |
|------|---|-----|
| 5.17 | Model calculated (solid line) and measured (experimental result) $\theta_s$ of TiAlN coating at $I = 5$ A, $S = 2050$ l/s and various substrate bias and nitrogen flow rate   | 149 |
| 5.18 | Model calculated (solid lines) and measured (experimental result) $\theta_s$ of TiAlN coating at unbiased substrate ( $V_b = 0$ ) and various nitrogen flow rate and its comparison with biased substrate of: (a) $V_b = -100$ V; (b) $V_b = -150$ V; (c) $V_b = -200$ V  | 150 |
| 5.19 | EDX of TiAlN coating composition at various nitrogen flow rate and substrate bias of: (a) -100 V; (b) -150 V; (c) -200 V  | 154 |
| 5.20 | EDX of TiAlN coating composition at various substrate bias and nitrogen flow rate of: (a) 30 sccm; (b) 60 sccm; (c) 65 sccm   | 156 |
| 5.21 | Interaction effect on Ti/Al ratio of TiAlN coating: (a) Ti/Al ratio vs nitrogen flow rate: triangle line curve is at high negatively substrate bias and the square line curve is at low negatively substrate bias; (b) Ti/Al ratio vs substrate bias: triangle line curve is at high nitrogen flow rate and the square line curve is at low nitrogen flow rate                      | 160 |
| 5.22 | Three dimension graph of Ti/Al ratio as function of substrate bias and nitrogen flow rate   | 161 |
| 5.23 | Interaction effect on Ti/(Ti+Al+N) ratio of TiAlN coating: (a) Ti/(Ti+Al+N) ratio vs nitrogen flow rate: triangle line curve is at high negatively substrate bias and the square line curve is at low negatively substrate bias; (b) Ti/(Ti+Al+N) ratio vs substrate bias: triangle line curve is at high nitrogen flow rate and the square line curve is at low nitrogen flow rate | 164 |
| 5.24 | Three dimension graph of Ti/(Ti+Al+N) ratio as function of substrate bias and nitrogen flow rate  | 165 |
| 5.25 | Model calculated (solid line) and measured (experimental result) deposition rate of TiAlN coating at $I = 5$ A, $S = 2050$ l/s and various substrate bias and nitrogen flow rate  | 170 |
| 5.26 | Deposition rate of TiAlN coating at various nitrogen flow rate and its comparison with biased substrate at: (a) $V_b = 0$ ; (b) $V_b = -100$ V; (c) $V_b = -150$ V; (d) $V_b = -200$ V  | 171 |
| 5.27 | SEM of TiAlN coating thickness at 65 sccm and substrate bias of: (a) -79 V; (b) -150 V; (c) -221 V<br>Magnification is 20000x and scale is in $1 \mu\text{m}$   | 174 |

|      |   |     |
|------|---|-----|
| 5.28 | SEM of TiAlN coating thickness at 60 sccm and substrate bias of: (a) 0 V; (b) -100 V; (c) -200 V<br>Magnification is 20000x and scale is in 1 $\mu\text{m}$                         | 175 |
| 5.29 | SEM of TiAlN coating thickness at 30 sccm and substrate bias of: (a) -100 V; (b) -150 V; (c) -200 V<br>Magnification is 20000x and scale is in 1 $\mu\text{m}$                      | 176 |
| 5.30 | TiAlN coating thickness at various nitrogen flow rate and substrate bias  | 177 |
| 5.31 | SEM of TiAlN coating thickness at -100 V and nitrogen flow rate of: (a) 30 sccm; (b) 60 sccm; (c) 70 sccm. Magnification is 20000x and scale is in 1 $\mu\text{m}$                  | 178 |
| 5.32 | SEM of TiAlN coating thickness at -150 V and nitrogen flow rate of: (a) 30 sccm; (b) 58 sccm; (c) 65 sccm; (d) 72 sccm. Magnification is 20000x and the scale is in 1 $\mu\text{m}$ | 179 |
| 5.33 | SEM of TiAlN coating thickness at -200 V and nitrogen flow rate of: (a) 30 sccm; (b) 60 sccm; (c) 70 sccm. Magnification is 20000x and scale is in 1 $\mu\text{m}$                  | 180 |
| 5.34 | SEM of TiAlN coating thickness at 0 V and nitrogen flow rate of: (a) 40 sccm; (b) 50 sccm; (c) 60 sccm<br>Magnification is 20000x and scale is in 1 $\mu\text{m}$ .                 | 181 |
| 5.35 | TiAlN coating thickness at various substrate bias and nitrogen flow rate  | 182 |
| 5.36 | XRD of Tungsten Carbide (WC) insert tool as substrate   | 186 |
| 5.37 | XRD of TiAlN coating at 65 sccm and various substrate bias  | 187 |
| 5.38 | XRD of TiAlN coating at 60 sccm and various substrate bias  | 188 |
| 5.39 | XRD of TiAlN coating at 30 sccm and various substrate bias  | 188 |
| 5.40 | Crystal plane spacing of TiAlN coating at various substrate bias and nitrogen flow rate of:<br>(a) 30 sccm; (b) 60 sccm; (c) 65 sccm  | 190 |
| 5.41 | Crystal size of TiAlN coating at various substrate bias and nitrogen flow rate of: (a) 65 sccm; (b) 60 sccm; (c) 30 sccm  | 192 |
| 5.42 | XRD of TiAlN coating at -100 V and various nitrogen flow rate   | 194 |
| 5.43 | XRD of TiAlN coating at -150 V and various nitrogen flow rate   | 194 |
| 5.44 | XRD of TiAlN coating at -200 V and various nitrogen flow rate   | 195 |
| 5.45 | XRD of TiAlN coating at 0 V and various nitrogen flow rate  | 195 |
| 5.46 | Crystal plane spacing of TiAlN coating at various nitrogen flow rate and substrate bias of:<br>(a) 0 V; (b) -100 V; (c) -150 V; (d) -200 V  | 197 |

|      |   |     |
|------|---|-----|
| 5.47 | Crystal size of TiAlN coating at various nitrogen flow rate and substrate bias of: (a) 0 V; (b) -100 V; (c) -150 V; (d) -200 V  | 199 |
| 5.48 | Crystal plane spacing of (111) TiAlN coating ( $d_{111}$ ) at 70 sccm and various substrate bias  | 203 |
| 5.49 | Three dimension graph of linear predictive model of $d_{111}$ as function of substrate bias and nitrogen flow rate  | 204 |
| 5.50 | (a) Effect of nitrogen flow rate on the crystal size of (111) TiAlN coating crystal at -200 V and various nitrogen flow rate; (b) effect of substrate bias on crystal size of (111) TiAlN coating ( $D_{111}$ ) at 70 sccm and various substrate bias | 207 |
| 5.51 | Three dimension of linear model predictive of $D_{111}$ TiAlN coating as function of substrate bias and nitrogen flow rate  | 208 |
| 5.52 | Optimum sputtering parameters to achieve the lowest $d_{111}$ of TiAlN coating  | 209 |
| 5.53 | TiAlN coating surface morphology at 65 sccm and substrate bias of: (a) -79 V; (b) -150 V; (c) -221 V  | 214 |
| 5.54 | TiAlN coating surface morphology at 60 sccm and substrate bias of: (a) -100 V; (b) -200 V   | 215 |
| 5.55 | TiAlN coating surface morphology at 30 sccm and substrate bias of: (a) -100 V; (b) -150 V; (c) -200 V   | 216 |
| 5.56 | Rms roughness of TiAlN coating at various nitrogen flow rate and substrate bias   | 217 |
| 5.57 | TiAlN coating surface morphology at -100 V and nitrogen flow rate of: (a) 30 sccm; (b) 60 sccm; (c) 70 sccm   | 218 |
| 5.58 | TiAlN coating surface morphology at -150 V and nitrogen flow rate of: (a) 30 sccm; (b) 58 sccm; (c) 65 sccm; (d) 72 sccm  | 219 |
| 5.59 | TiAlN coating surface morphology at -200 V and nitrogen flow rate of: (a) 30 sccm; (b) 60 sccm; (c) 70 sccm   | 220 |
| 5.60 | Rms roughness of TiAlN coating at various substrate bias and nitrogen flow rate   | 221 |
| 5.61 | Rms roughness of TiAlN coating at 65 sccm and various substrate bias  | 224 |
| 5.62 | Three dimension graph of rms roughness of TiAlN coating as function of substrate bias and nitrogen flow rate  | 225 |
| 5.63 | Force vs indentation depth of TiAlN coating at various substrate bias and nitrogen flow rate of: (a) 65 sccm; (b) 60 sccm; (c) 30 sccm  | 231 |
| 5.64 | TiAlN coating hardness at various nitrogen flow rate and substrate bias   | 232 |

|      |   |     |
|------|---|-----|
| 5.65 | Force vs indentation depth of TiAlN coating at various nitrogen flow rate and substrate bias of: (a) -100 V; (b) -150 V; (c) -200 V   | 233 |
| 5.66 | TiAlN coating hardness at various substrate bias and nitrogen flow rate   | 234 |
| 5.67 | TiAlN coating hardness at 65 sccm and various substrate bias  | 238 |
| 5.68 | Three dimension graph of TiAlN coating hardness as function of substrate bias and nitrogen flow rate  | 239 |
| 5.69 | Lateral crack diameter vs applied load for TiAlN coating at various substrate bias and nitrogen flow rate of: (a) 30 sccm; (b) 60 sccm; (c) 65 sccm   | 245 |
| 5.70 | Slope measurement of TiAlN coating at various nitrogen flow rate and substrate bias   | 246 |
| 5.71 | Lateral crack diameter vs applied load of TiAlN coating at various nitrogen flow rate and substrate bias of: (a) -100 V; (b) -150 V; (c) -200 V   | 247 |
| 5.72 | Slope measurement of TiAlN coating at various substrate bias and nitrogen flow rate   | 248 |
| 5.73 | Interaction effect on slope. Triangle line and square line are high level and low level of nitrogen flow rate, respectively   | 252 |
| 5.74 | Three dimension graph of slope as functions of substrate bias and nitrogen flow rate  | 253 |
| 5.75 | Optimum sputtering parameters to achieve lowest slope   | 254 |
| 5.76 | Interaction effect on commercially TiAlN coating flank wear at $f = 0.4$ mm/rev. Square and triangle lines indicate a low and a high level of depth of cut, respectively                      | 261 |
| 5.77 | Three dimension graph of quadratic predictive equation of commercially TiAlN coating flank wear at feed rate of 0.3 mm/rev as function of cutting speed and depth of cut                      | 262 |
| 5.78 | Optical microscope of commercially TiAlN coating flank wear at: (a) $f = 0.4$ mm/rev, $v = 468$ m/min, $a = 0.4$ mm; (b) $f = 0.4$ mm/rev $v = 300$ m/min, $a = 0.4$ mm. Magnification is 50x | 263 |
| 5.79 | Optimum cutting conditions to achieve the lowest flank wear   | 264 |
| 5.80 | Surface roughness at: (a) $v = 300$ m/min, $a = 0.4$ mm and various feed rate; (b) $f = 0.4$ mm/rev, $a = 0.4$ and various cutting speed  | 267 |
| 5.81 | Surface roughness contours at various feed rate and cutting speed and depth of cut of: (a) 0.5 mm; (b) 0.3 mm   | 269 |
| 5.82 | Three dimension model of linear predictive equation of surface roughness at depth of cut 0.5 mm and various feed rate and cutting speed   | 270 |

|       |   |     |
|-------|---|-----|
| 5.83  | Optimum condition to achieve lowest surface roughness   | 271 |
| 5.84  | Optimum condition to achieve lowest flank wear and surface roughness  | 273 |
| 5.85  | Optical microscopy of TiAlN coating flank wear at various substrate bias and nitrogen flow rate of: (a) 70 sccm; (b) 65 sccm; (c) 60 sccm. Magnification is 50x | 277 |
| 5.86  | TiAlN coating flank wear at various nitrogen flow rate and substrate bias   | 278 |
| 5.87  | Optical microscopy of TiAlN coating flank wear at various nitrogen flow rate and substrate bias of: (a) -100 V; (b) -150 V; (c) -200 V. Magnification is 50x    | 279 |
| 5.88  | TiAlN coating flank wear at various nitrogen flow rate  | 280 |
| 5.89  | TiAlN coating flank wear at: (a) N <sub>2</sub> flow of 65 sccm and various substrate bias; (b) substrate bias of -150 V and various nitrogen flow rate         | 283 |
| 5.90  | Three dimension graph of TiAlN coating flank wear as function of substrate bias and nitrogen flow rate  | 284 |
| 5.91  | Three dimension graph of surface roughness as function of substrate bias and nitrogen flow rate   | 286 |
| 5.92  | Correlation of flank wear and hardness of TiAlN coating   | 290 |
| 5.93  | Correlation of flank wear and adhesion strength of TiAlN coating  | 291 |
| 5.94  | Correlation of flank wear and (111) crystal plane spacing of TiAlN coating  | 291 |
| 5.95  | Correlation of flank wear and rms roughness of TiAlN coating surface  | 292 |
| 5.96  | Correlation of flank wear and composition of TiAlN coating: (a) Ti content; (b) Al content; (c) N content   | 294 |
| 5.97  | Correlation of flank wear and thickness of TiAlN coating  | 295 |
| 5.98  | Correlation of adhesion strength and d <sub>111</sub> of TiAlN coating  | 296 |
| 5.99  | Correlation of hardness and adhesion strength of TiAlN coating  | 297 |
| 5.100 | Correlation of hardness and (111) crystal plane spacing of TiAlN coating  | 298 |
| 5.101 | Correlation of hardness and roughness of TiAlN coating  | 299 |
| 5.102 | Correlation of hardness and thickness of TiAlN coating  | 300 |
| 5.103 | Correlation of adhesion strength and thickness of TiAlN coating   | 301 |
| 5.104 | Correlation of adhesion strength and composition of TiAlN coating: (a) Ti content; (b) Al content; (c) N content  | 302 |